ISSN 2231-346X (Print)
JUSPS-A Vol. 29(10), 456-467 (2017). Periodicity-Monthly
Section A
ISSN 2319-8044 (Online)

JOURNAL OF ULTRA SCIENTIST OF PHYSICAL SCIENCES
An International Open Free Access Peer Reviewed Research Journal of Mathematics
website:- www.ultrascientist.org
Estd. 1989

Non-Similar Unsteady Flow in the Stagnation Region of a Vertical Plate Due to Impulsive Motion

SHANKAR RAO MUNJAM[1*]

[1*] School of Naval Architecture, Ocean and Civil Engineering
Shanghai Jiao Tong University, Shanghai, Minhang, 200 240 (China)
* Corresponding Author Email: munjam.shankarrao11@gmail.com
http://dx.doi.org/10.22147/jusps-A/291006

Acceptance Date 9th September, 2017, Online Publication Date 2nd October, 2017

Abstract

In this paper, an approximate analytical solution is obtained for the unsteady mixed convection flow near the stagnation region of a heated vertical plate. The unsteadiness in the flow field is caused by impulsively creating motion in the free stream and at the same time suddenly raising the surface heat flux above its surroundings. This study gains importance when the buoyancy forces due to the temperature difference between the surface and the free stream become large. The Homotopy Analysis Method (HAM) is applied to solve the coupled system of non linear partial differential equations for analytical solutions. The numerical results of the flow are computed using the Keller-Box Method (KBM). A detailed error analysis is performed to compute the total average squared residual errors for velocity and temperature. It is shown that a more accurate solution can be obtained with least computational effort by the computed approximate analytical series solution of velocity and temperature.

Keywords: Non-similar; Impulsive motion; Stagnation point; KBM; HAM for PDE.
MSC Code: 35C10, 35Q79, 65Nxx, 80M25, 97N80.

Introduction

The study of mixed convection (combination of free and forced convection) flow over a semi-infinite vertical plate has received considerable research interest due to its industrial and technical applications in solar receivers exposed to wind currents, electronic devices cooled by fans.

The two-dimensional stagnation point flow in a mixed convection refers to the flow in the vicinity of a stagnation line that result from a two-dimensional flow impinging on a surface at right angles and flowing there after symmetrically about the stagnation line. Consequently, both the flow and temperature are significantly

affected by the buoyancy forces.

The importance of studying the unsteady non-similar boundary layer flow near stagnation region is that, the heat transfer is maximum near the stagnation region. In many problems the flow may be unsteady which might be caused by the change in the free stream velocity or in the surface temperature (surface heat flux) or in both. When there is an impulsive change in the velocity field, the inviscid flow is developed instantaneously, but the flow in the viscous layer near the wall is developed slowly which becomes fully developed steady flow after sometime. For lower time the flow is dominated by the viscous forces and the unsteady acceleration, but for large time it is dominated by the viscous forces, the pressure gradient and the convective acceleration. For lower time the flow is generally independent of the conditions far upstream and at the leading edge or at the stagnation point and for large time the flow depends on these conditions. Thus, unsteadiness influences the flow and heat transfer to a great extent.

There are several studies related to flow near stagnation region in the literature. To list a few related to the present study, the unsteady mixed convection flow near stagnation region of a heated vertical plate with thermal dissipation effects has been investigated by Alharbi *et al*.[1]. Beg *et al*.[2] presented the cross-diffusion effects on mixed convection, heat and species transfer boundary layer flow due to a inclined plate numerically.

The unsteady, mixed convection flow near the stagnation point on vertical plate in a two-dimensional flow has been studied by the authors Kumari *et al*.[7] Lok *et al*.[11] and Ramachandran *et al*.[13]. The two-dimensional non-similarity boundary layer flow has been investigated under different aspects by Kousar *et al*.[6], Liao[8,9,10], Motsa[12] and Seshadri *et al*.[14].

Recently, Shafie *et al*.[16] studied the non-similarity boundary layer flow including the effect of thermophoresis and injection/suction in the stagnation point with micropolar fluid due to a moving plate and given numerical solution using implicit finite difference method. Srinivasacharya *et al*.[17] presented the natural convection flow of non-similar solution with effect of thermophoresis and Brownian motion due to a doubly stratified porous medium and solved the governing equations numerically using a Keller-Box method. This method was initially introduced by Keller *et al*.[5] and subsequently this idea was further exposed by Cebeci *et al*.[3].

Two-dimensional unsteady, boundary layer flow near the stagnation region of a flat plate has been studied by Williams *et al*.[18]. Two-dimensional non similar boundary layer flow near a stagnation region has been solved analytically by Xu *et al*.[19] and You *et al*.[20]. Two-dimensional similarity boundary layer flow of non-Newtonian incompressible viscoelastic fluid due to a continuous stretching surface has been solved analytically by Seshadri *et al*.[15]. The highly nonlinear differential equation has been solved with help of ADM and HAM by Elsaid[4]. But in all the above research papers cited there is no analytical solution for the flow and temperature of the mixed convection flow due to impulsive motion near the stagnation region. Moreover, the application of HAM to non linear coupled partial differential equations to obtain analytical form of solutions is not done by many researchers. Hence, the present study is significant in using advanced HAM procedure to compute an approximate analytical solution to coupled non linear partial differential equations.

This paper is outlined as follows. In Section 2, the aim of study is presented. We consider the problem formulation and governing equations in Section 3. In Section 4, we describe the standard HAM solution procedure for solving the present non-linear partial differential equations (PDEs). Along the way, in Section 5, the procedure of Keller-Box Method (KBM) solving for PDEs is presented. We shall make several observations on study variables and physical parameters in the solution series, and some of these summarized in the results and discussion, which are presented in Section 6. Finally, we presented conclusion in Section 7.

Present Study :

The aim of this paper is to study the development of flow and heat transfer near the stagnation region in the presence of buoyancy forces over a heated vertical plate. The unsteadiness in the flow field is caused by impulsively creating motion in the free stream and at the same time suddenly raising the surface temperature (heat flux) above its surroundings. The problem is formulated in such a way that at $t = 0$ it is represented by the Rayleigh type of equation and for $T \to T_\infty$ it is represented by the Hiemenz type of equation. The partial differential equations governing the flow and the heat transfer have been solved analytically using the HAM and numerically by Keller Box Method. Particular cases of the present results are compared with those of Seshadri *et al.*[14]. HAM solutions are always represented as a power series form in which the coefficients contain the study parameters. In our analysis the various study parameters considered are the buoyancy parameter (λ), Unsteadiness in the flow (t) and Prandtl number (Pr). We have also computed the numerical solutions for our governing equations using Keller-Box method (KBM).

Problem Formulation and Governing Equation :

Consider a semi-infinite vertical plate which is placed in an ambient fluid with uniform temperature T_∞. At $t = 0$ the fluid is impulsively moved with a velocity U_e and at the same time the surface temperature or heat flux is suddenly raised. Figure 1 show a flow field over a heated vertical surface where the upper half of the flow field is assisted by the buoyancy force, but the lower part is opposed by the buoyancy force. The reverse trend appears if the plate is cooled from below. The results illustrated here are valid for both cases. The surface of the plate is assumed to have an arbitrary temperature or it is subjected to an arbitrary heat flux. Under the above assumptions and considering Boussinesq approximations, the unsteady laminar boundary layer equations governing the mixed convection flow are given by Ramachandran *et al.*[13].

$$u_x + v_y = 0, \tag{1}$$

$$u_t + uu_x + vu_y = U_e(U_e)_x + \upsilon u_{yy} + g\alpha(T - T_\infty) \tag{2}$$

$$T_t + uT_x + vT_y = \beta T_{yy} \tag{3}$$

The initial conditions for the problem when $t < 0$ are:

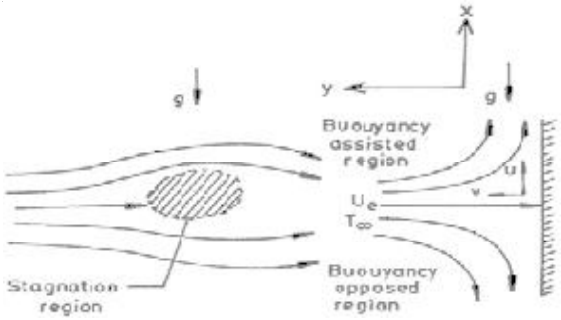

FIGURE 1. The coordinate system of flow model.

$$u(x, y) = v(x, y) = 0, \qquad T(x, y) = T_\infty. \tag{4}$$

The boundary conditions for the problem when $t \geq 0$ are:

$$u(x, y) = v(x, y) = 0, u(x, \infty) = U_e = ax, a > 0.$$

$$T(x, \infty) = T_\infty, \qquad T(x, 0) = T_w(x) = bx^n, \; b > 0, \; n \geq 0, \tag{5}$$

for the prescribed surface temperature (PST case) and

$$-k\frac{\partial T(x,0)}{\partial y} = q_w(x) = cx^n,\ c > 0, \tag{6}$$

for the prescribed surface heat flux (PHF case).

The indices n = 1 and n =0 correspond the linear surface temperature and the co- nstant surface temperatures, respectively.

Here x and y are distances along and normal to the surface, respectively, u and v are the components of the velocity along the x-and y-directions, respectively. T, k, v, q_w, α, g and β are the temperature, thermal conductivity, kinematic viscosity , surface heat transfer, coefficient of volumetric thermal expansion, the gravitational fluid acceleration and the thermal diffusivity, respectively; Subscripts e, ∞ and w are the conditions at the edge of the boundary layer, at the free stream and in the surface, respectively. The subscripts t, x and y denote the derivatives with respect to the t, x and y, respectively.

It is worth mentioning here that we encountered certain difficulties in formulating the boundary layer problem in the presence of impulsive motion. We used the scaling of $Q = y/(tv)^{\frac{1}{2}}$ t*=u_et/x for small-time solution as well as for large-time solution for the scale $\eta = yu_e/(vx)^{\frac{1}{2}}$. If the boundary layer problem is formulated in (Q, t*)-system, the small-time solution fits in properly, but the large-time solution does not fit. Therefore we have to find a scaling of the y coordinate which behaves like $y/(tv)^{\frac{1}{2}}$ for small-time solution and as $yu_e/(vx)^{\frac{1}{2}}$ for large-time solution. Then it was realized that if we take the time scale ξ then the region of time integration may become finite. Such transformations has been reported by the author Seshadri *et al.*[14] as follows.

$$\eta = y\left(\frac{a}{v}\right)^{\frac{1}{2}}(\xi)^{-\frac{1}{2}},$$
where $\xi = 1 - e^{-t^*},\ t^* = at,\ a > 0,$
$u(x,y,t) = ax F'(\eta,\xi),$
$v(x,y,t) = -(av)^{1/2}(\xi)^{1/2} F(\eta,\xi)$ and
$T(x,y,t) = T_\infty + (T_w - T_\infty)G(\eta,\xi).$

(PST Case)

$$T(x,y,t) = T_\infty + \left(\frac{a}{v}\right)^{-\frac{1}{2}}(q_w/k)G(\eta,\xi).$$

(PHF Case).

Substituting these similarity transformations into (2)–(3), we find that (1) is identically satisfied and (2)-(3) are reduced to the following system of non-linear partial differential equations.

$$F''' + 2^{-1}\eta(1-\xi)F' + \xi\,(1-(F')^2 + FF'' + \lambda G) - \xi(1-\xi)\frac{\partial F'}{\partial \xi} = 0, \tag{7}$$

$$G'' + 2^{-1}\eta(1-\xi)G'Pr + \xi(FG' - nF'G)\,Pr - Pr\,\xi(1-\xi)\frac{\partial G'}{\partial \xi} = 0. \tag{8}$$

The boundary conditions (5) reduces to,

$F(0,\xi) = F'(0,\xi) = 0,\ F'(\infty,\xi) = 1, G(0,\xi) = 1,\ G(\infty,\xi) = 0.$ (PST Case)

$G'(0,\xi) = -1.$ (PHF Case) (9)

Here F' is the dimensionless velocity. F and G are the dimensionless stream function and temperature, respectively and prime denotes derivative with respect to η, and the constants are

$\Pr = \frac{\upsilon}{\beta}$, $Re_x = \frac{\alpha x^2}{\upsilon}$. $\lambda = \frac{Gr_x}{Re_x{}^2}$. (PST Case) and $\lambda = \frac{Gr^*_x}{Re_x{}^{5/2}}$ (PHF Case), where $Gr_x = g\alpha(T_w - T_\infty)x^3/v^3$ and $Gr^*_x = g\alpha q_w x^4/kv^3$.

Where Pr is the Prandtl number, λ is the buoyancy parameter, $\mathrm{Re_x}$ is the local Reynolds number, η is the pseudo-similarity variable and a, b and c are the constants; t and t* are the dimensional and dimensionless times, respectively; Gr_x and Gr^*_x are the Grashof numbers for the PST and PHF cases, respectively.

It can be seen that the buoyancy parameter λ is the function of stream wise distance x unless the surface temperature $T_w - T_\infty$ and the surface heat flux q_w vary linearly with x (i.e., n = 1). For n = 1, λ is constant. In particular, $b = c = \alpha g a^2$, then λ = 1. Hence for the self-similar solution both $T_w - T_\infty$ and q_w should vary linearly with x (i.e., n = 1). For $n \neq 1$ the equations are locally self-similar.

The local Skin friction coefficient on the surface in terms of the shear stress can be expressed as

$$C_f = \frac{2\mu}{\rho U_e{}^2}\left(\frac{\partial u}{\partial y}\right)_{y=0}$$

$$= 2(\xi \mathrm{Re_x})^{-1/2} F''(0,\xi), \qquad \xi > 0.$$

The heat transfer coefficients in terms of the Nusselt number for PST and PHF cases are

$$Nu = \frac{x}{(T_w - T_\infty)}\left(\frac{\partial T}{\partial y}\right)_{y=0}$$

$$= (\mathrm{Re_x})^{\frac{1}{2}}\left[(\xi)^{-1/2}/G(0,\xi)\right], \qquad \xi > 0.$$

Without loss of generality, we substitute $F = U, G = V, \xi = t$ and $h = x$ into (7)-(9) and rewrite the equations as follows. The renaming of these variables is in par with the physical meanings of the variable and to match our Mathematica program variables and its outputs. It is done purely for our convenience.

$$U_{xxx} + 2^{-1}x(1-t)U_{xx} + t(1-(U_x)^2 + UU_{xx} + \lambda V) - t(1-t)(U_x)_t = 0, \quad (10)$$

$$V_{xx} + 2^{-1}x(1-t)V_x\Pr + t(UV_x - nU_xV)\Pr - t\Pr(1-t)(V_x)_t = 0. \quad (11)$$

The boundary conditions (5) reduces to,

$$U(0,t) = U_x(0,t) = 0,\ U_x(\infty,t) = 1$$

$$V(0,t) = 1,\ V(\infty,t) = 0.\ \text{(PST Case)}\ V_x(0,t) = -1.\ \text{(PHF Case)} \quad (12)$$

Equations (10) and (11) are coupled nonlinear parabolic partial differential equations and the corresponding boundary conditions are given by (12). These equations for n=1(steady case) are identical to those of Ramachandran *et al.*[13]. Also (10) under conditions (12) for buoyancy parameter λ = 0 (forced convection flow) is the same as that of Williams *et al.*[18] when m=1 in their equations.

HAM Solution :

The main components of the HAM procedure are selecting suitable initial profiles satisfying the

boundary conditions of the problem; choosing an appropriate Initialguess and linear operators as

$$U_0(x,t) = 1 - e^{-x} \text{ and } V_0(x,t) = e^{-x}, \tag{13}$$

$$L_U = U_{xxx} - U_x;\ L_V = V_{xx} - V, \tag{14}$$

so that its solutions are simpler to evaluate analytically. The nonlinear operator is directly written from the governing equation of the problem. In HAM analysis, we always get a system of deformation equations which have to be solved.

A detailed HAM procedure and error analysis (Ref. Seshadri et al. (2014)). The results are presented as

$$U_l(x,t;\ c_U) = \Omega_l U_{l-1}(x,t;\ c_U) + U_l^*(x,t;\ c_U) + C_1^l + C_2^l e^x + C_3^l e^{-x} \tag{15}$$

$$V_l(x,t;\ c_V) = \Omega_l V_{l-1}(x,t;\ c_V) + V_l^*(x,t;\ c_V) + C_4^l e^x + C_5^l e^{-x}. \tag{16}$$

When $l = 1$ in (15) and (16), the solution series are computed as

$$U_1(x,t) = 1 - e^{-x} + x + \frac{c_U}{2} - \frac{7tc_U}{2} + \lambda t c_U + \left(\frac{c_U}{2} - \frac{xc_U}{2}\right)e^{-x} + \left(\frac{7c_U}{2} + \frac{xc_U}{2} - \lambda c_U\right)te^{-x}. \tag{17}$$

$$V_1(x,t) = e^{-x} + c_V - \frac{c_V Pr}{2} - \frac{3tnPrc_V}{2} + \left(c_V - \frac{Prc_V}{2} + \frac{xPrc_V}{2}\right)e^{-x} - tPrc_V. + \left(\frac{3Prc_V}{2} + \frac{3nPrc_V}{2} - \frac{xPrc_V}{2}\right)te^{-x} \tag{18}$$

In the similar way, we can obtain the series solution for $U_2(x,t)$, $V_2(x,t)$ and $U_3(x,t)$, $V_3(x,t)$ and so on. Since the series solution expressions are too long to be fitted in a page even for $U_2(x,t)$ and $V_2(x,t)$ they are not given here. From these series solutions form, it can be seen that the number of terms in the series solutions grows very large as *l* increases from 2 to 3. One can imagine the size of the series for $l = 10$, such large size calculations can be handled with ease using Mathematica. In all of the figures, we use $\lambda = n = t = 1$, $c_U = -1.63203$, $c_V = -0.45538$ and Pr=0.7 unless it is mentioned otherwise.

Numerical Solution :

Though several numerical results are available in the literature, to compare our own approximate analytical results for various parametric values, we have performed numerical computation with the simple and still popular technique Keller-Box Method (KBM). The numerical solution of (10) and (11) subject to the boundary conditions are obtained using the KBM. Since the details of KBM can be got from the recent work of Shafie[16] and Srinivasacharya *et al.*[17], it is not given here. Briefly mentioning, we first reduce the governing non dimensional equations to a first order system; the system obtained is then approximated using central differences. The resultant difference equations are linearized by Newton's method. The final tri-diagonal systems are then solved using Varga's Algorithm.

The numerical results and approximate analytical results agree very well in all the calculations, some of which they are shown in the tables.

Result and Discussion

We have studied the effect of various parameters such as Prandtl number Pr, Buoyancy parameter λ and unsteady parameter t on velocity and temperature profiles as well as on skin friction and heat transfer rates for both PST and PHF cases. The approximate analytical solutions are obtained in the form of a general series for both the velocity U(x,t) and the temperature V(x,t) after solving the governing equations with its appropriate boundary conditions using the computational software Mathematica. The expressions for U(x, t) and V(x, t) have been computed up to 30th-order.

The convergence of the non-similar HAM series solutions strongly depends on the convergence

control parameters c_U and c_V which control the rate of convergence. It is customary in HAM analysis to plot c_U and c_V-curves to identify the interval of optimal convergence control parameters within which any value can be chosen to obtain convergent of the non-similar HAM solution.

The HAM-based Mathematica package BVPh.2 has been used to compute the minimum value of the total average squared residual errors of governing equations. The total average squared residual attained its minimum values at $c_U = -1.63203$, $c_V = -0.45538$ and these values are used for all computation of our results. We have convergent non-similarity HAM series solutions for governing equations in the whole domain $0 < t < 1$ and $0 < x < +\infty$. These calculations, not only give the efficiency region of the convergence control parameters but also their appropriate values to enable faster convergence of the non-similar HAM series solutions.

Computations have been carried out for several combinations of parameters λ, t and Pr, and some representative results are presented here in the form of Tables 1-3 and Figure 3-13.

It can be seen in Table 1 that as we increase the order of iteration the corresponding minimum of the average squared residual errors decreases. Also observed the CPU time to compute the exact residual errors even for the lesser order of approximation. For example it needs 25.04, 372.44, 835.62, 1023.25 and 1723.15 seconds of CPU time for l = 1,5,10,15,30 respectively and therefore not very useful in practice. The computation is stopped when a certain convergence criterion is satisfied. Tables 2 and 3 present the convergence of surface shear stress $U''(0, t)$ and heat transfer rate $V'(0, t)$ for the PST and PHF cases when t=0.5 and $\lambda = n = 1$ at various values of Prandtl numbers. Numerical calculations are done using Keller-Box Method (KBM) to compute velocity and temperature for various values of the dimensionless parameters of the problem. Numerical results of present HAM and KBM are compared in Tables 2 and 3 and are found to be in good agreement.

The c_U and c_V curves have been drawn for the 10^{th}-order non-similar solution series for different values of unsteady parameter t such as t = 0.0, 0.5 and 1.0 which are shown in Figure 2. It is seen that at t = 0.0 and 1.0, shear stress rates $U''(0, t)$ converges to the values for all c_U in the interval [-1.9, -0.3] and [-1.5, -0.0], respectively. At t = 0.5, it also converges to the same value (which is different from that at t = 0.0 and 1.0) when in the interval [-2.1, -0.4]. However, at t = 0.5, $U''(0, t)$ converges in the region [-2.1, -0.4]. Similarly, at t = 0 and 1.0, the heat transfer rate $-V'(0, t)$ converges to the values for all c_V in the interval [-1.9, -0.3] and [-1.6, -0.2], respectively. At t = 0.5, it also converges to the values (which is different from that at t = 0 and 1.0) when in the interval [-1.3, -0.2]. However, at t = 0.5, $-V'(0, t)$ converges in the region [-1.3, -0.2].

Table 1. Minimum of the average squared residual error E_U and E_V with the CPU time(Sec.) at different order of iterations for Pr = 0.7 and t = n = λ = 1 by using $c_U = -1.63203$ and $c_V = -0.45538$

ℓ	E_U	E_V	CPU time(sec.)
1	1.646122×10^{-4}	1.094900×10^{-3}	25.04
5	1.867819×10^{-5}	$1{:}784361\times10^{-4}$	372.44
10	2.092342×10^{-6}	$3{:}002289\times10^{-5}$	835.62
15	4.109238×10^{-7}	$2{:}338722\times10^{-6}$	1023.25
20	3.228370×10^{-8}	$5{:}931709\times10^{-7}$	1289.88
25	2.356275×10^{-9}	$1{:}777216\times10^{-8}$	1501.06
30	1.209200×10^{-10}	$1{:}074358\times10^{-9}$	1723.15

Table 2. The shear stress rate U" (0, t) and heat transfer rate $-V'(0, t)$ for the PST case when t = n = 1

		U" (0, t)		$-V'(0, t)$	
Pr	λ	HAM	KBM	HAM	KBM
0.7	1	1.78181	1.78182	1.09499	1.09500
7.0	1	1.59513	1.59513	1.79373	1.79375
20.0	1	1.49738	1.49739	2.51995	2.51999
60.0	1	1.41685	1.41685	3.52916	3.52916
0.7	-1	0.72629	0.72630	0.79108	0.79109
7.0	-1	0.95669	0.95673	1.58257	1.58251
20.0	-1	1.11155	1.11159	2.32438	2.32437
60.0	-1	1.22744	1.22746	3.30649	3.30649

Therefore, c_U in the interval [-1.6, -0.4] does not affect the values of shear stress rates and c_V is [-1.5, -0.3] for heat transfer rate. To answer to the question as to which optimum values of c_U and one has to choose in these intervals, the computation of average squared residual errors has the answer. It helps to obtain the optimal value of these optimal convergence control parameters within that interval.

The variation of the skin friction coefficients (i.e., $2^{-2}(\mathrm{Re}_x)^{1/2} c_f$) and the Nusselt number (i.e. $2^{-2}(\mathrm{Re}_x)^{1/2} \mathrm{Nu}$) with t for the PST case when Pr = 0.7, 7.0 are shown in Figure 3. It observed that, the increase in unsteady parameter t decreases the both skin friction and heat transfer, which means that the boundary layer thickness decreases with increasing unsteady parameter. Due to the impulsive motion the skin friction and the heat transfer coefficients have large values for small time after the start of the motion and they decrease continuously and reach the steady-state values at t=1 ($t^* \to \infty$).

Table 3. The shear stress rate U" (0, t) and heat transfer rate $-V'(0, t)$ for the PHF case when t = n = 1

		U" (0, t)		$-V'(0, t)$	
Pr	λ	HAM	KBM	HAM	KBM
0.7	1	1.42964	1.42968	1.14646	1.14646
7.0	1	1.39860	1.39860	1.63280	1.63287
20.0	1	1.32140	1.32140	2.45475	2.45475
60.0	1	1.28246	1.28248	3.51652	3.51652
0.7	-1	0.78391	0.78390	1.08767	1.08767
7.0	-1	1.08172	1.08175	1.52549	1.52550
20.0	-1	1.19559	1.19559	2.40008	2.40009
60.0	-1	1.23501	1.23503	3.45576	3.45576

The influence of the shear stress $U''(0, t)$ and heat transfer rate $-V'(0, t)$ with t for the PST case when $\lambda = 0,5,10$ (the buoyancy assisting case) at fixed Pr = 0.7 are plotted in Figure 4. Here, the shear stress and the heat transfer rates increase with λ, because positive buoyancy force acts like favourable pressure gradient which accelerates the motion and reduces both momentum and thermal boundary layers. Therefore, both the shear stress and the surface heat transfer rates are increased. For t=n = 1.0 and Pr = 0.7, the shear stress and heat transfer rates increase by about 49 % and 43%, respectively, as λ increases from 0 to 10. Also, the heat transfer rate $-V'(0, t)$ for n = 0.0, 1.0, $\lambda = 0,5,10$ at fixed Pr = 0.7 are plotted in Figure 4. For n = 0 (isothermal surface

case), the heat transfer is found to be less (about 37%) than that of n = 1 (non-isothermal surface case). The reason for this trend is that for n = 0 the surface temperature difference $T_w - T_\infty$ is less than that for the case of n = 1. This results in lower heat transfer for n = 0 as compared to n = 1. Also, for gases ($\mu\alpha T$) reduction in surface temperature causes thinner boundary layer which in turn increases the shear stress rates.

The effect of unsteadiness on the velocity and temperature profiles U'(x, t) and V(x, t) when $\lambda = n = 1$ and Pr = 0.7 are plotted in Figure 5-6. Here, the velocity increases and temperature decreases with increasing the unsteady parameter t. The effect of buoyancy parameter λ on the velocity and temperature profiles are plotted in Figure 7-8. It is seen that both velocity and temperature increases for λ = 1.0,0.0, –0.5,–1.0 for a fixed unsteady parameter and for the isothermal surface case.

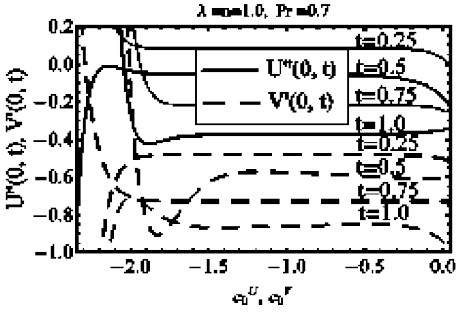

FIGURE 2. Curves of the 10th-order approximation of $U''(0, t)$ and $-V'(0, t)$ when t = 0, 0.5 and 1.0.

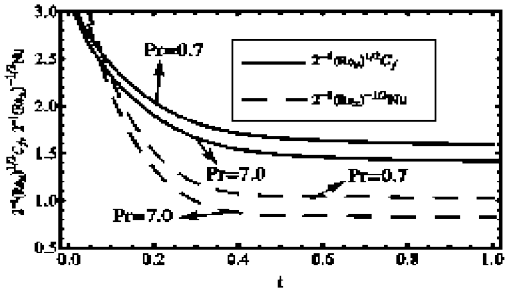

FIGURE 3. Variation of the skin friction coefficient and Nusselt Number with t for the PST case when λ =1, n = 1, Pr = 0.7 and 7.0.

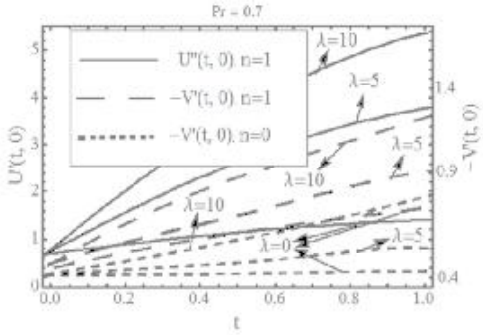

FIGURE 4. Variation of the shear stress and heat transfer rates with t for the PST case when λ=0, 5, 10 and n = 0, 1at Pr =0.7.

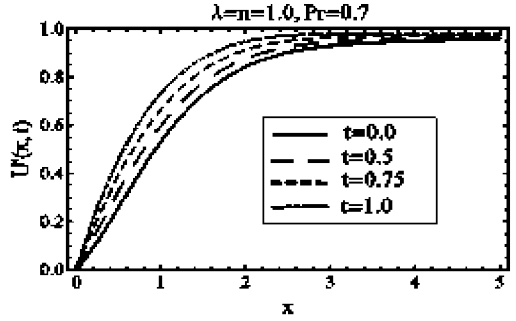

FIGURE 5. Velocity profiles for various values of t.

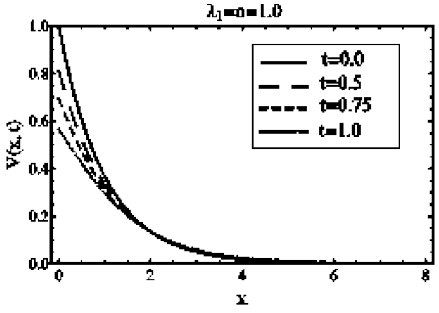

FIGURE 6. Temperature profiles for various values of t.

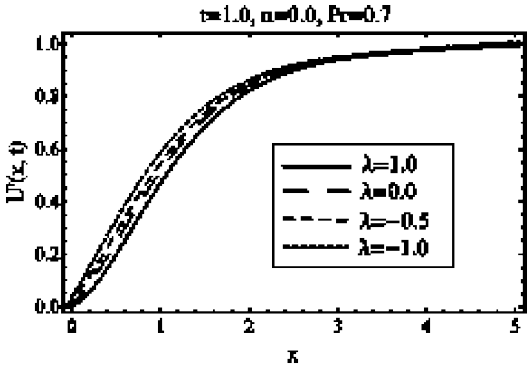

FIGURE 7. Velocity profiles for various values of λ.

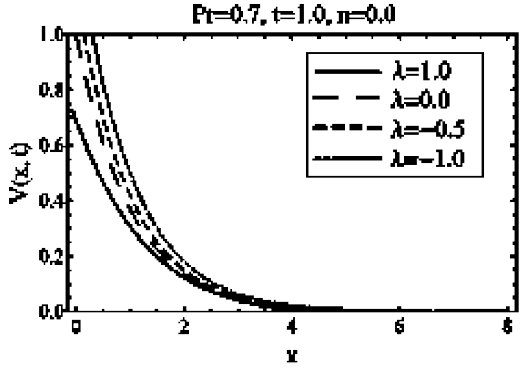

FIGURE 8. Temperature profiles for various values of λ.

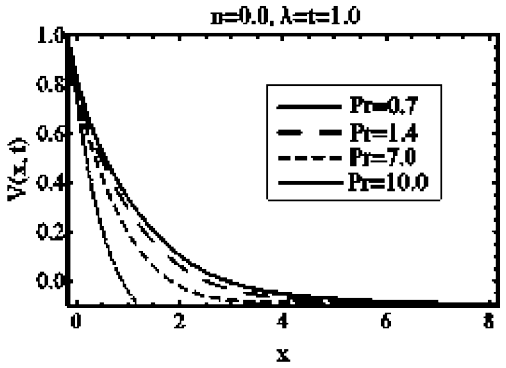

FIGURE 9. Temperature profiles for various values of Pr.

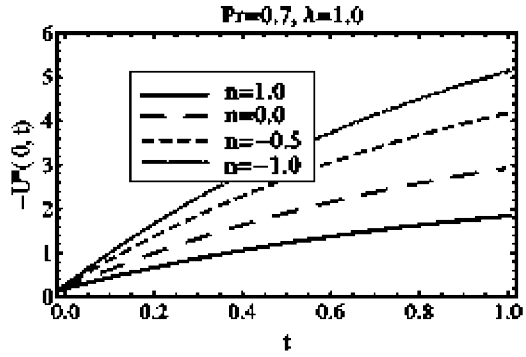

FIGURE 10. Effect of t on -U" (0, t) for different values of n for the PST case.

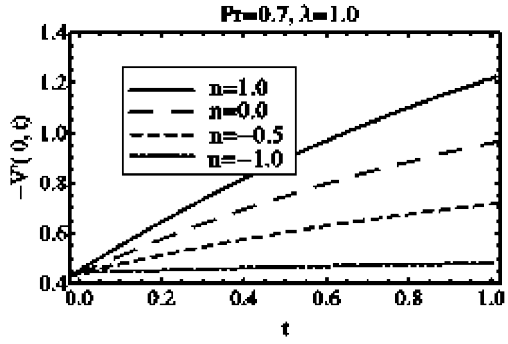

FIGURE 11. Effect of t on -V'(0, t) for different values of n for the PST case.

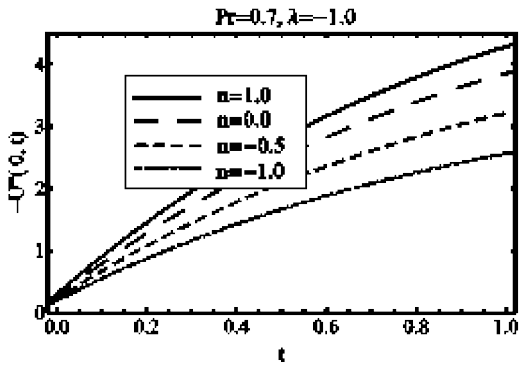

FIGURE 12. Effect of t on -U"(0, t) for different values of n for the PHF case.

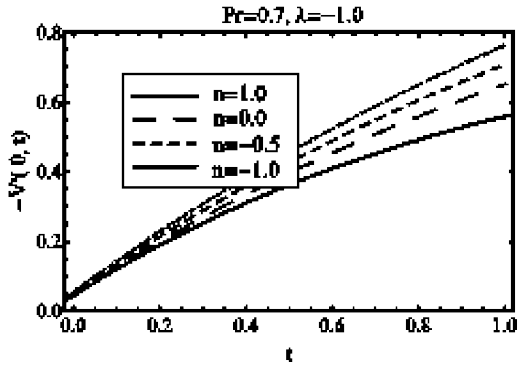

FIGURE 13. Effect of t on -V' (0, t) for different values of n for the PHF case.

The effect of Prandtl number Pr on the temperature profiles V(x, t) for the PST case is displayed in Figure 9. This demonstrates the fact that the temperature profiles decrease with the increase of Pr. Physically, Pr=0.7 and 7.0, correspond to air and water respectively. Since the increase in the Pr from 0.7 to 10 reduces the

thermal boundary layer, the temperature profiles decrease with increasing Pr. Also for large Pr the thermal boundary layer is much thinner than the momentum boundary layer, because the effect of Pr is more pronounced on the temperature profiles than on the velocity profiles. This is due to the fact that Pr occurs explicitly in the energy equation.

The surface shear stress -U"(0, t) and heat transfer rate -V'(0, t) for n =1.0, 0.0, -0.5, -1.0 with t for the PST and PHF cases corresponding buoyancy flow $\lambda > 0$ and $\lambda < 0$ at fixed Pr = 0.7 are plotted in Figures 10-13. It is observed that the shear stress increases and the heat transfer rate decreases with decreasing n values. For buoyancy assisting flow $\lambda > 0$, the shear stress and heat transfer rates for the prescribed surface heat flux are slightly less than those of the prescribed surface temperature, but for the buoyancy opposing flow $\lambda < 0$ the reverse trend is observed.

Conclusion

The present study discusses the development of flow and heat transfer near the stagnation region in the presence of buoyancy forces over a heated vertical plate. The solutions have been obtained for flow and heat transfer in the form of the series solution using an advanced Homotopy analysis method (HAM) while the numerical results are computed using the Keller-Box Method (KBM). The surface shear stress and heat transfer are found to be increasing with time and there is a smooth transition from the small-time solution to the large-time solution. The surface shear stress and heat transfer for buoyancy assisting flow are more than those of the buoyancy opposing flow. The surface shear stress decreases for the buoyancy assisting flow and increases for the buoyancy opposing flow. For buoyancy assisting flow, the surface shear stress and heat transfer for the prescribed surface heat flux are slightly less than those of the prescribed surface temperature, but for the buoyancy opposing flow the reverse trend is observed. The surface heat transfer can considerably be reduced by using a lower Prandtl number fluid. It can also be reduced by imposing the buoyancy force in the opposite direction to that of the forced flow or by maintaining uniform temperature. The accuracy and efficiency of the proposed methods have been demonstrated by the numerical results. This approach has general meanings and thus can be used to solve many same types of coupled system of non linear partial differential equations in science and engineering.

Acknowledgement

The author gratefully acknowledges support of the Shanghai Jiao Tong University, Government of China through the Post Doctoral Fellowship (Reg. No. 179838).

References

1. Alharbi, S. M., Hassanien, I. A., Unsteady Mixed Convection Flow in the Stagnation Region of a Heated Vertical Plate Embedded in a Variable Porosity Medium with Thermal Dispersion Effects. *INTECH Open Access Publisher* (2013).
2. Beg, O. A., Bakier, A., Prasad, R., Ghosh, S. K., Numerical modelling of non-similar mixed convection heat and species transfer along an inclined solar energy collector surface with cross diffusion effects. *World Journal of Mechanics 1,* 185 (2011).
3. Cebeci, T., Bradshaw, P. (1984). *Physical and computational aspects of convective heat transfer*. Springer Science and Business Media (2011).
4. Elsaid, A., Adomian polynomials: A powerful tool for iterative methods of series solution of nonlinear equations. *Journal of Applied Analysis and Computation 2,* 381-394. (2012).
5. Keller, H. B., Cebeci, T. , Accurate numerical methods for boundary layer flows. Part I, Two dimensional

laminar flows. *In Proceedings of the second International conference on numerical methods in fluid dynamics*. Springer Berlin Heidelberg, 92-100 (1971).
6. Kousar, N., Mahmood, R., Series solution of non-similarity boundary- layer flow in porous medium. *Applied Mathematics 4,* 127 (2013).
7. Kumari, M., Nath, G., Development of mixed convection flow over a vertical plate due to an impulsive motion. *Heat and mass transfer 40,* 823-828 (2004).
8. Liao, S. J., An analytic solution of unsteady boundary-layer flows caused by an impulsively stretching plate. *Communications in Nonlinear Science and Numerical Simulation 11,* 326-339 (2006).
9. Liao, S. J., (2009). A general approach to get series solution of non-similarity boundary-layer flows. *Communications in Nonlinear Science and Numerical Simulation 14,* 2144-2159 (2006).
10. Liao, S. J., *Homotopy analysis method in nonlinear differential equations*. Berlin: Springer (2012).
11. Lok, Y. Y., Amin, N., Pop, I., Unsteady mixed convection flow of a micropolar fluid near the stagnation point on a vertical surface. *International journal of thermal sciences 45,* 1149-1157 (2006).
12. Motsa, S. S., On the practical use of the spectral homotopy analysis method and local linearization method for unsteady boundary-layer flows caused by an impulsively stretching plate. *Numerical Algorithms 66,* 865-883 (2014).
13. Ramachandran, N., Chen, T. S., Armaly, B. F., Mixed convection in stagnation flows adjacent to vertical surfaces. *Journal of Heat Transfer 110,* 373-377 (1988).
14. Seshadri, R., Sreeshylan, N., Nath, G., Unsteady mixed convection flow in the stagnation region of a heated vertical plate due to impulsive motion. *International Journal of Heat and Mass Transfer 45,* 1345-1352 (2002).
15. Seshadri, R., Munjam, S. R., The study of Heat and Mass Transfer in a Visco elastic fluid due to a continuous stretching surface using Homotopy Analysis Method. *Journal of Applied Analysis and Computation 4,* 389-403 (2014).
16. Shafie, S., Unsteady MHD stagnation-point flow with heat and mass transfer in a micropolar fluid in the presence of thermophoresis and suction/injection}. *Indian Journal of Pure and Applied Mathematics 44,* 729-741 (2013).
17. Srinivasacharya, D., Surender, O., Non-similar solution for natural convective boundary layer flow of a nanofluid past a vertical plate embedded in a doubly stratified porous medium. *International Journal of Heat and Mass Transfer 71,* 431-438 (2014).
18. Williams, III, J. C., Rhyne, T. B., Boundary layer development on a wedge impulsively set into motion. *SIAM Journal on Applied Mathematics 38,* 215-224 (1980).
19. Xu, H., Liao, S. J., Pop, I., Series solutions of unsteady boundary layer flow of a micropolar fluid near the forward stagnation point of a plane surface. *Acta Mechanica 184,* 87-101 (2006).
20. You, X., Xu, H., Homotopy solution for non-similarity boundary-layer flow near a stagnation point. *Zeitschrift für Naturforschung A 65,* 161-172 (2010).